TÉCNICO LISBOA

Radio Pulsar Navigation System

João Maia Tomé

Thesis to obtain the Master of Science Degree in

Electrical and Computer Engineering

Supervisors: Professor Jorge Manuel dos Santos Ribeiro Fernandes
Doctor Diogo Rodrigues Oliveira de Brito

Examination Committee

Chairperson: Professor Teresa Maria Canavarro Menéres Mendes de Almeida
Supervisor: Professor Jorge Manuel dos Santos Ribeiro Fernandes
Member of the Committee: Professor Gonçalo Nuno Gomes Tavares

November 2022

Declaration

I declare that this document is an original work of my own authorship and that it fulfils all the requirements of the Code of Conduct and Good Practices of the Universidade de Lisboa.

Acknowledgments

Firstly, I would like to give a very special thanks to both of my supervisors, Professor Jorge Fernandes and Doctor Diogo Brito, for their time, support and knowledge in developing this work. I am grateful for the opportunity to work in a project thesis of this area.

I am also grateful to Instituto Superior Técnico (IST) and INESC-ID for the facilities and conditions that permitted the continuous development of this thesis.

The work developed in this thesis was also supported by FCT, Fundação para a Ciência e a Tecnologia (Portugal), under the projects UIDB/50021/2020, UNSEEN - PTDC/EEI-EEE/31416/2017; and FCT/EU Moore4Medical - H2020-ECSEL-2019-IA-876190.

I would also like to thank my family and friends for supporting me throughout my academic studies. Especially my parents and my brother, who continuously give me strength to reach my goals.

Abstract

Navigation systems have been of common use for the past decades, but their development has been essential throughout history to map and locate new areas, as well as, moving safely between them. Currently, most of these systems rely on the Global Navigation Satellite Systems (GNSS), more specifically the Global Positioning System (GPS).

However, these systems are not suitable outside their orbital sphere, inhibiting localization in outer space. Other navigation systems need to be explored for this application and that is what NASA and ESA are doing. The use of Pulsars is one of the new methods being explored, with the use of their extremely precise, unique and periodic signals. These signals have very weak power when received on Earth, lower than the noise level itself. Meaning that specialized hardware is required.

With that, in this thesis, the partial development of a receiver suitable for this application is explored, using a quadratic receiver topology. More specifically, a 1 GHz frequency Gilbert cell mixer, with a switching current bias, and a relaxation oscillator implemented on a 65 nm CMOS technology. The oscillator has a frequency of 106 kHz, with an output amplitude of 0.6 V, centered at 1.9 V. The final circuit, simulated, obtained a constant output gain of 4.5 dB at the application frequencies, a bandwidth of 7.3 GHz, with a 1dB compression point of -9.5 dBm.

Keywords

Navigation System, Pulsar, Receiver, Mixer, Relaxation, Oscillator.

Resumo

Nas últimas décadas, os sistemas de navegação têm sido de uso bastante comum, mas o seu desenvolvimento foi essencial ao longo da história para mapear e localizar novas áreas, assim como, deslocar-se em segurança entre elas. Atualmente, a maioria destes sistemas depende dos Sistemas Globais de Navegação por Satélite (GNSS), mais especificamente o Sistema de Posicionamento Global (GPS).

No entanto, estes sistemas não são adequados fora da órbita terrestre, impossibilitando assim o seu uso no espaço. Dessa forma, sistemas de navegação diferentes precisam de ser explorados para esta aplicação, estando a NASA e a ESA a explorar nesse sentido. A utilização de pulsares tem surgido como uma possibilidade, devido aos seus sinais precisos, únicos e periódicos. Porém, estes sinais têm uma baixa potência, mais baixa do que o próprio nível de ruído, quando recebidos em Terra. Isto implica a utilização de hardware especializado.

Nesta tese, foi feito o desenvolvimento parcial de um recetor adequado para essa aplicação, utilizando uma topologia recetora quadrática. Mais especificamente, um misturador de frequência baseado na célula de Gilbert de 1 GHz, com uma corrente de polarização comutada, e um oscilador de relaxação numa tecnologia CMOS de 65 nm. O oscilador tem uma frequência de 106 kHz, com uma amplitude de saída de 0,6 V, centrada a 1,9 V. O circuito final, simulado, obteve um ganho de saída constante de 4,5 dB nas frequências de aplicação, uma largura de banda de 7,3 GHz, com um ponto de compressão de 1dB a -9,5 dBm.

Palavras Chave

Sistema de Navegação, Pulsar, Receptor, Misturador, Relaxação, Oscilador.

Contents

List of Tables

List of Figures

Acronyms

AC	Alternate Current
ADC	Analog-to-Digital Converter
DC	Direct Current
DSN	Deep Space Network
ESA	European Space Agency
ESTRACK	European Space Tracking
FFT	Fast Fourier Transform
FOM	Figure of Merit
GNSS	Global Navigation Satellite Systems
GPS	Global Positioning System
IF	Intermediate Frequency
LNA	Low-Noise Amplifier
LO	Local Oscillator
LTCC	Low-Temperature co-Fired Ceramics
MOSFET	Metal–Oxide–Semiconductor Field-Effect Transistor
NASA	National Aeronautics and Space Administration
NF	Noise Figure
RF	Radio Frequency
SNR	Signal-to-Noise Ratio
SSB	Solar System Barycenter
TOA	Time of Arrival
VCO	Voltage-Controlled Oscillator

1

Introduction

Contents

Introduction

1.1 Motivation

Navigation is always accompanied by a means of localization. Throughout history this has evolved from the simple use and memorization of constellations that allowed to monitor the cardinal points, to the use of equipment, such as the astrolabe, to precisely determine the positions of these constellations.

Such methods of localization are always connected to a mapping system, allowing for the adjustment and measurement of the distance to the desired point, while also giving a detailed route that can be used.

These navigation systems have gone from physical maps used with compasses, later-on substituted by the astrolabe and the sextant. Which became obsolete or used only as a backup system due to the technological advancements in the last century, these have become obsolete, being replaced by the Global Navigation Satellite Systems (GNSS) with the common use worldwide of the Global Positioning System (GPS). Although very precise and extremely versatile on Earth, their utilization is limited to just that, the Earth. The satellites used are not available in outer space, meaning that navigation outside earth is not possible with such systems.

For outer space, spacecrafts currently rely on the observation of stars, with a base station on Earth acting as an observer, a reference and determining the route to be taken. This means that travelling in deep space is limited by the communication of the base station and the spacecraft, which currently are based radio and radar systems for both European Space Agency (ESA) European Space Tracking (ESTRACK) and National Aeronautics and Space Administration (NASA) Deep Space Network (DSN) [1].

The objective of this thesis is to make a specific component of an optimum receiver, shown in Figure 1.1, envisioned in [2] where a navigation system is proposed for outer space autonomous navigation using pulsars.

1.2 Objective

The main focus of this work is to develop the mixer (MXR) envisioned in the quadratic receiver topology proposed in Brito's PhD dissertation [2], with the LO also being developed as a consequence. The whole proposed topology can be seen in Figure 1.1, with the section developed in this thesis highlighted in the dashed square in red.

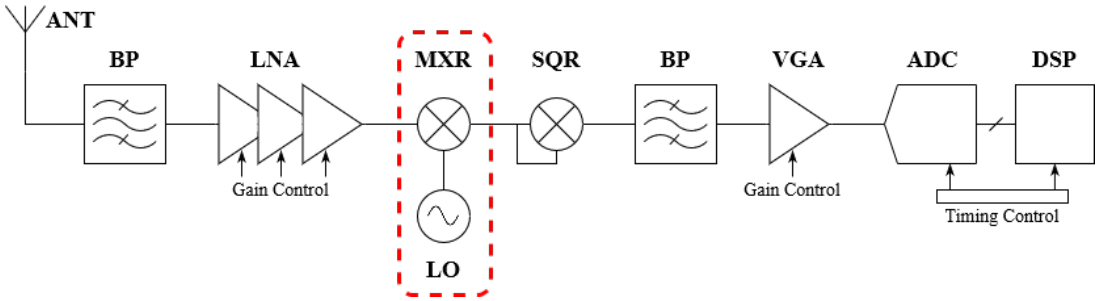

Figure 1.1: Proposed quadratic receiver topology in [2].

As such, the goal for this thesis is to develop a mixer for signals with a bandwidth of around 400 MHz at a center frequency of 1 GHz that will be used in the pulsar receiver, as well as, the 100 kHz oscillator that will be connected to the LO port of the mixer. For this, the TSMC65N technology is used on the Cadence tool for development and simulation purposes.

1.3 Document organization

This work is organized as follows:

- This chapter, is an introduction for navigation systems and the need of new methods for outer space localization, as well as, what the thesis consists.
- Chapter 2 shows the necessary background along with the state of the art theory in pulsars and mixers. In this chapter some of the work already published in the areas of receivers and localization using pulsars is also presented.
- Chapter 3 the development of the circuits is presented, as well as, a summary of the decision making and considerations for the proposed circuits.
- Chapter 4 presents the simulation results of the presented circuits.
- In Chapter 5 the final thesis conclusions are presented and possible future work is proposed.

2

Background and Related Work

Contents

Background and Related Work

2.1 Pulsar

Pulsars are pulsating stars, more specifically rapidly rotating neutron stars which magnetization emits beamed radio and other high energy radiation (X-ray to gamma-ray). These were firstly discovered on November 1967, by Jocelyn Bell Burnell, with the discovery of a radio emitting pulsar named ”PSR B1919+21”. The radiation and the periodicity of pulsars' rotation makes their use ideal for navigation in deep space, especially with some specific pulsars [2]. This is a relatively new topic, with challenging means of detection, but that also means that new sources are discovered regularly.

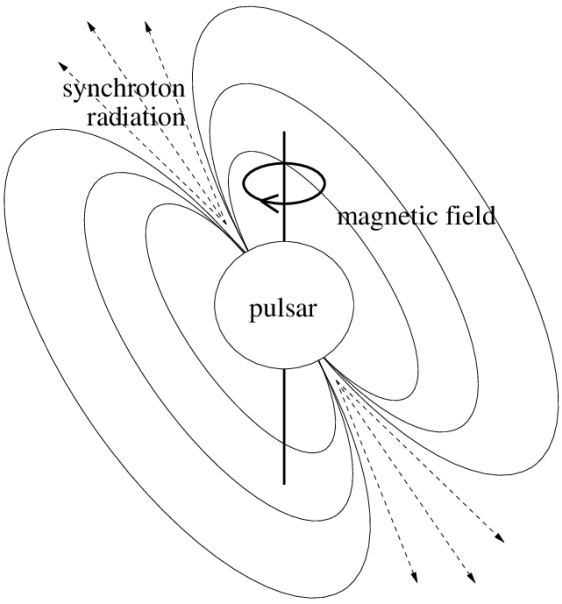

Figure 2.1: Pulsar model [3].

2.1.1 Pulsar Physics

What makes them exceptional for navigation and timing is their rotational period, which allows the extraction of extremely precise time of arrival (TOA) of radio signals, challenging even that of the atomic clocks' timing precision [4]. The main pulsars for this usage are those where the axis of rotation does not match the axis of radiation. That allows, just like a lighthouse, the radiation beam to be detected periodically. Luckily, about 90% of the known pulsars are in this category, with about 7% being millisecond pulsars, with periods ranging from 1.5 to 30 ms [5]. Millisecond pulsars are pulsars with companion stars, gradually building up mass and angular momentum, decreasing the magnetic field and therefore maintaining its millisecond period for billions of years [6]. These are the desirable pulsars for navigation, not only for their longevity, but because their position, relative to the Solar System Barycenter (SSB), can be acquired precisely in less time, as there are more pulses for the same time frame compared to other pulsars. Currently there are about 530 of these pulsars registered in the "ATNF Pulsar Catalogue" [7].

To obtain the TOA, we must first have an understanding of the pulsar rotation. The rotational phase of the pulsar in relation to a given time t is given by

$$\phi(t) = \phi(t_0) + f(t - t_0) + \tfrac{1}{2}\dot{f}(t - t_0)^2 + ... \tag{2.1}$$

with rotational frequency as

$$f = \frac{d\phi}{dt}, \tag{2.2}$$

where t_0 is a given reference epoch, and $\dot{f}$ is the first derivative of f [8]. This lets us determine the minor deviations on the pulse timing compared to the expected signal timing from the SSB and adjust the TOA.

2.1.2 Pulsar Signal

The challenging aspect of using pulsars for navigation is the detection of their signal (pulse). Thankfully, each pulsar has a unique profile, allowing the distinction between them. Even though the pulsar signals are extremely precise and stable, there can be some variation between pulses observed from the same source [9], but by averaging and folding, the correct profiles can be obtained, as shown in Figure 2.2. The known profiles are of high precision, allowing to accelerate the time it takes to identify a specific pulsar signal, by means of correlation.

The signal is challenging to detect due to the low power that is received at the detector. This means that the pulses are undetectable with a single sample, as the noise is at a higher power level than the pulse itself. In order to improve their detection, several techniques can be employed at hardware level, such as low noise receivers to maximize the already low Signal-to-Noise Ratio (SNR) and at a post-

processing level, as mentioned above, by employing folding with the desired time periods and with the aid of correlation in case there are several pulsar signals mixed in the receiver. These techniques are mainly used for the observation and detection of new pulsars.

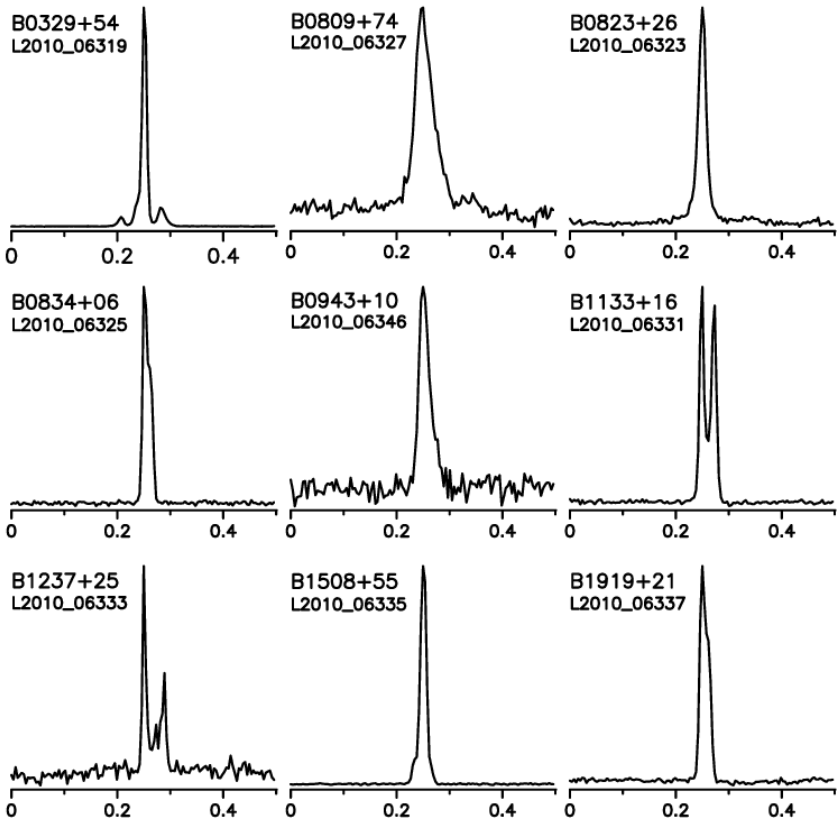

Figure 2.2: Pulse profile for nine different pulsars [10].

The signal of the pulsar, at the source, can be mathematically perceived using the model presented in (2.3) [11]. The model for the signal is

$$s_p(t) = a(t) \cdot p(t) = a(t) \cdot \sum_{n=-\infty}^{\infty} p(t - nT_p), \tag{2.3}$$

having the pulsar signal as two separate components, $a(t)$ which is a natural random process, in this case a zero-mean real Gaussian, caused by the synchrotron radiation, and the deterministic signal $p(t)$ which is related to the pulsars rotation at period T_p. Figure 2.3 is a representation of these signals. Since $a(t)$ is stationary, this results in a cyclo-stationary pulsar signal, with an average period of T_p.

Having understood the model of the signal, the important aspects to acquire the signal are the SNR and the frequency spectrum. In relation to the latter, pulsars have a wide range of frequencies, with the most likely candidates in the radio frequencies, X-rays or γ-rays. The use of the high energy pulsars like the X-ray and γ-rays seems logical, since it improves the SNR, but not only are the receivers more

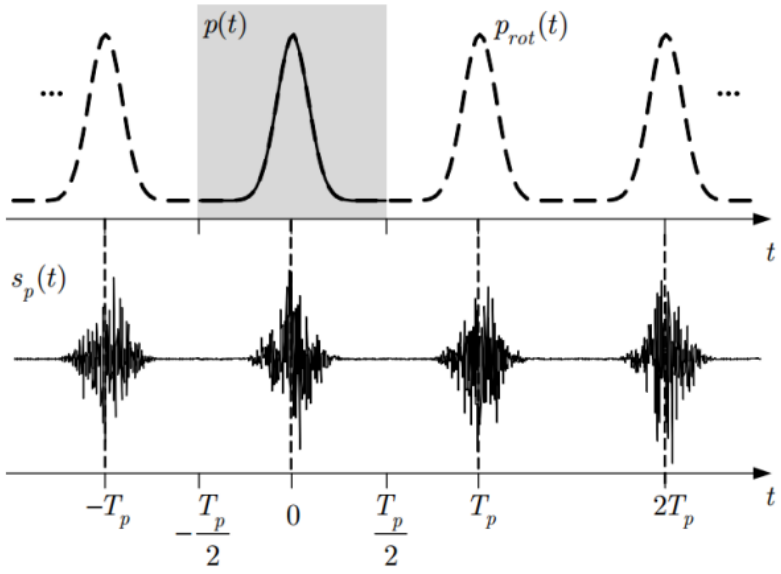

Figure 2.3: Graphics of the model for $s_p(t)$ and $p(t)$ [11].

complicated and unpractical [12], these pulsars represent only a small portion of the known pulsars to date, with the first γ-ray pulsars only being discovered recently [13]. Radio frequency pulsars are more common, with easier topologies for the receivers, but that comes at a loss of the SNR.

To determine the SNR, the power and the noise of the pulsar signal at the receiver need to be analyzed. Since the signal is below noise level, the antenna size is of extreme importance, as the power at the receiver is directly proportional to the antenna size. Taking this into account, the signal power at the receiver (S_i) is given by:

$$S_i = \alpha \cdot A_e \cdot 10^{-26} S_i' \left(\frac{f_{rec}}{f_{ref}}\right)^{\beta_i} \cdot B, \qquad \text{[W]} \quad (2.4)$$

where α is the polarization parameter of the signal, which in itself can aid in the navigation system, with the calibration of the receiver orientation [14]. As mentioned before, the power is proportional to the antenna size A_e (m^2), S_i' (Jy) is the i-th pulsar flux at the reference frequency f_{ref} (Hz), usually $f_{ref} = 1$ GHz, f_{rec} (Hz) is the receiver center frequency, β_i is the pulsar spectral index and B (Hz) is the receiver bandwidth. The factor 10^{-26} is to convert the reference pulsar flux from Jansky unit to $\mathrm{W\,m^{-2}\,Hz^{-1}}$.

For the noise, this is influenced by the location of the receiver and the environment it's in. The receiver noise (S_n) can be determined by:

$$S_n = k_B \cdot (T_{rec} + T_{back} + T_{galaxy} + T_{solar}) \cdot B, \qquad \text{[W]} \quad (2.5)$$

where k_B is the Boltzmann constant, $k_B = 1.380649 \cdot 10^{-23}$ (J K^{-1}), T_{rec} (K) is the receiver noise temperature, $T_{back} = 2.7$ K is the background noise temperature of the Cosmos, $T_{galaxy} = 6 f_{rec}^{-2.2}$ (K) is the background temperature noise of the galaxy and $T_{solar} = (72 \cdot f_{rec} + 0.058) \cdot A_e \cdot 10^{A_{sl}/10} \cdot d^{-2}$ (K) is the noise temperature of the solar system, affected by the sun $(72 \cdot f_{rec})$ and Jupiter (0.058), where d (AU) is the distance between the receiver and the sun and A_{sl} (dB) is the attenuation of the antenna main side lobe.

Therefore, according to [11], from equations 2.4 and 2.5, the SNR is given by:

$$SNR = \frac{S_i}{S_n} = \frac{\alpha \cdot A_e \cdot 10^{-26}}{k_B (T_{rec} + 2.7 + 6 f_{rec}^{-2.2} + (72 \cdot f_{rec} + 0.058) \cdot A_e \cdot 10^{A_{sl}/10} \cdot d^{-2})} \cdot S_i' \left(\frac{f_{rec}}{f_{ref}} \right)^{\beta_i} \quad (2.6)$$

where the factor

$$S_i' \left(\frac{f_{rec}}{f_{ref}} \right)^{\beta_i} \quad (2.7)$$

is solely pulsar dependent, while the rest is receiver dependent.

2.1.3 Pulsar Receiver

Taking into consideration the SNR obtained from 15 suitable radio frequency pulsars, as shown in Figure 2.4, the center frequency of the receiver is best around the 1 GHz mark [11], to maximize the SNR, since most of the pulsars peak around that frequency. Even with this, the desired signal of all the pulsars is well below the -40 dB mark compared to the noise.

Once again, this is a big hurdle for the detection of pulsar signals. The need to detect signals below the noise level leads to the development of low-noise receivers, used in conjunction with several data processing techniques. As mentioned before, this thesis focuses on the quadratic receiver topology proposed by Brito. This architecture focuses on the use of a squarer after the initial low-noise amplifier (LNA), which allows the small bandwidth of the received signal (pulsar signal and noise) to be squared and shifted to the direct current (DC) region. The advantage of this methodology, since the signal bandwidth is in the few hundreds of kHz, is the possibility of using a better performing Analog-to-Digital Converter (ADC), with a reduced sampling frequency and high resolution, which is one of the most important features of the architecture.

An issue with the usage of a squarer is the appearance of unwanted noise. This is caused by flicker noise near DC, where the output signal of the squarer is expected to be, therefore increasing the system noise and negatively impacting the system sensitivity. In order to circumvent this limitation, the implementation of a frequency mixer in conjunction with a LO is proposed [2]. With a LO frequency slightly above the usual pulsar signal bandwidth, which is lower than 100 kHz for most pulsars [2]. The

signal is then squared, however, since it was slightly shifted, the pulsar profile is no longer in the DC region, but still at a few hundred kHz. More specifically, at two times the LO frequency.

Since this thesis focuses on this part of the receiver, in the next section, the functionality and technological advancements of mixers are presented.

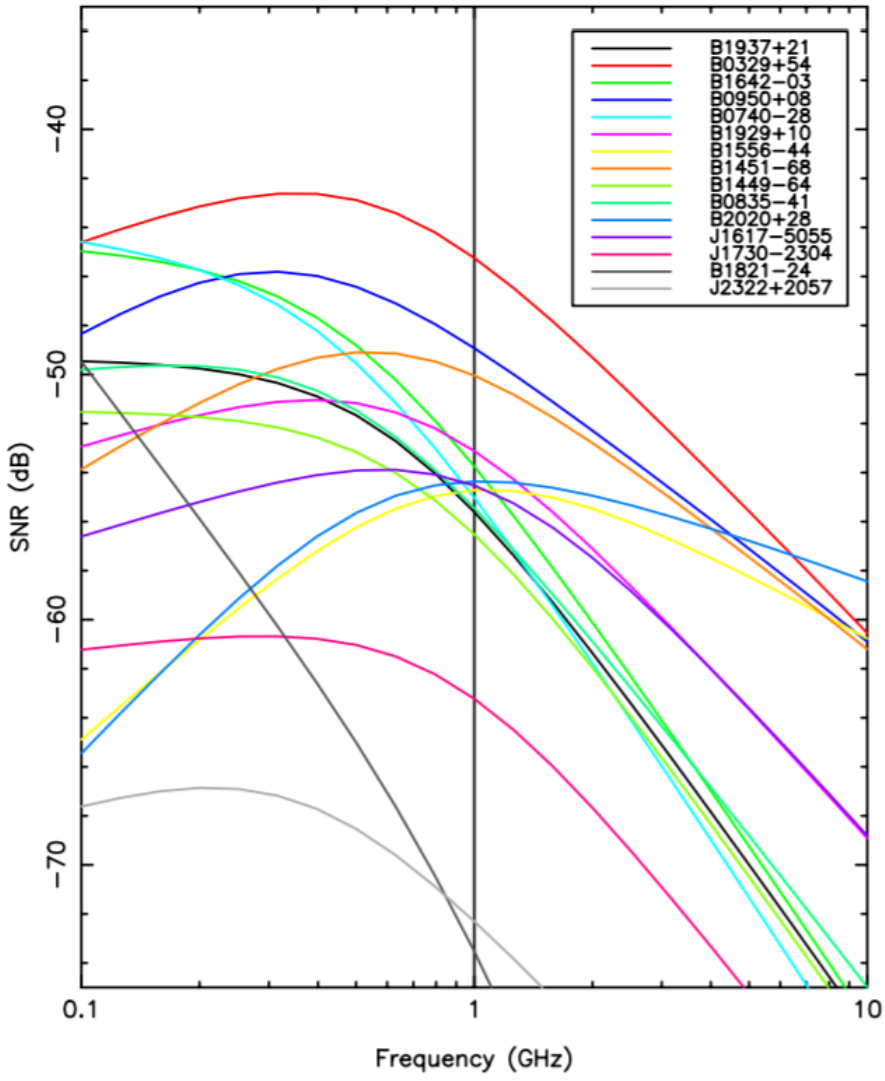

Figure 2.4: SNR as a function of frequency for 15 pulsars, with $A_e = 10$ m^2 [15].

2.2 Mixers

Mixers are an essential building block for a receiver. Their function is to perform frequency translation by multiplying two waveforms.

In their basic form, frequency mixers are composed of three distinct ports: radio frequency (RF), LO and intermediate frequency (IF). When used as a down-conversion mixer, the RF port is the input signal, the LO port is where the oscillator is connected and the IF port is the output with the two frequencies mixed.

One way to categorize different mixers is based on the circuitry used. They can be passive or active. Passive mixers use passive components, or active components in a passive region, for the switching element in the RF part, such as diodes or saturated transistors. They are known as switching mixers and don't consume any DC power. Their use is limited by their inability to have gain, since there is no transconductance stage, and their limited frequency response. As for active mixers, these use transistors, in a transconductance stage, and can provide gain as well as the mixing of the two signals. However, the noise figure (NF) is higher than in a passive mixer.

Since the transconductance stage is the major contributor for non-linearity, passive mixers are not affected by it, since even if they have metal–oxide–semiconductor field-effect transistor (MOSFET) transistors as switches, they are ideally in the triode region. This means that, usually, passive mixers have better linearity than active mixers.

Mixers can also be categorized by whether they are single-balanced or double-balanced. Non-balanced mixer, or single-ended mixers, are not used in current day RF circuits, since half of the LO period is not used [16]. Figure 2.5 presents a non-balanced mixer, where if the LO voltage is not high enough (e.g negative half cycle of a sinusoidal signal) to activate the transistor, the output is not grounded and not reflective of the input.

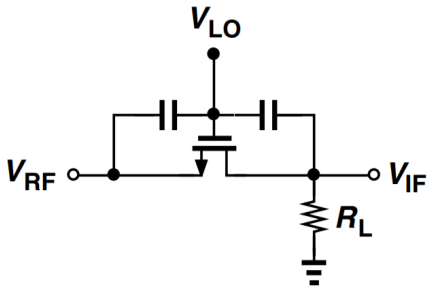

Figure 2.5: Example of basic single-ended mixer [17].

2.2.1 Mixer Metrics

In order to compare different mixers, the Figure of Merit (FOM) in (2.8) is useful to have an idea of the relative performance taking into consideration the most important aspects of the mixer [18]. The FOM for mixers is given by:

$$FOM = 10 \cdot \left(\frac{10^{G_c/20} \cdot 10^{(\text{IIP3}-10)/20}}{10^{\text{NF}/10} \cdot P_{MIX}(\text{mW}) \cdot 10^{-3}} \right), \tag{2.8}$$

where (G_c) is the mixer's conversion gain, IIP3 is its input third-order intercept point, NF is the noise factor of the mixer and P_{MIX} is the mixer power.

Conversion gain (G_c) is the power (or voltage, current, etc) gain between the input and output signals of the mixer. In the case of a down-conversion mixer, it is

$$G_c = \frac{P_{IF}(f_{IF})}{P_{RF}(f_{RF})}. \tag{2.9}$$

Another important metric is the conversion gain compression, more specifically the 1 dB compression point. This is the input power point where the output signal starts showcasing amplitude distortion and the mixer loses its linearity. The 1_{dB} compression point is defined as the input RF power required to have a conversion loss of 1 dB from ideal [19].

The third-order intercept point (IP3) is accepted as an important parameter for mixer performance. It's a mathematical construct that is used to predict nonlinear behavior when the input power increases and is defined as "It is the extrapolated point where the fundamental and third order inter-modulation products (IM3) intersect each other. At this point, $\text{IM}_3 = 0$ dBc". This can be roughly interpreted as the power at which the third order products are at the same power as the carrier.

NF is the the fraction between input SNR at the input frequency and output SNR at the output frequency, as follows:

$$\text{NF} = \frac{\text{SNR}_{in}}{\text{SNR}_{out}}. \tag{2.10}$$

2.2.2 Single-Balanced and Double-Balanced Mixers

As mentioned before, one way to categorize frequency mixers is if their inputs and outputs are balanced or not. Firstly, the notion of a single-balanced mixer is explained, with examples of its possible implementation as a passive or active circuit. Afterwards, double-balanced mixers and their possible active and passive implementations are presented.

A single-balanced mixer consists of a single differential switching pair. As shown in Figure 2.6(a), the LO drives the switching pair and therefore modulates the input voltage for the passive circuit. In case of the active circuit (Figure 2.6(b)), the LO also drives the switching pair, but since it is using transistors, it is modulating the tail current that resulted from the conversion of the RF signal at the transconductance stage. This means that the multiplication of the two signals is done in the current domain. Since the obtained output for both cases is differential (benefit of a balanced mixer), RF feedthrough from LO to IF is nullified [16].

Since the single-balanced mixer has fewer active components than the double-balanced counterpart, its NF is also lower. The addition of an inductor at the source of M_4 of Figure 2.6(b) will improve the linearity of the circuit. This can be further improved if instead of a degenerated source, there was a common gate transconductance stage, but this would not attenuate the noise from the switching pair, causing the circuit to be relatively noisier [20].

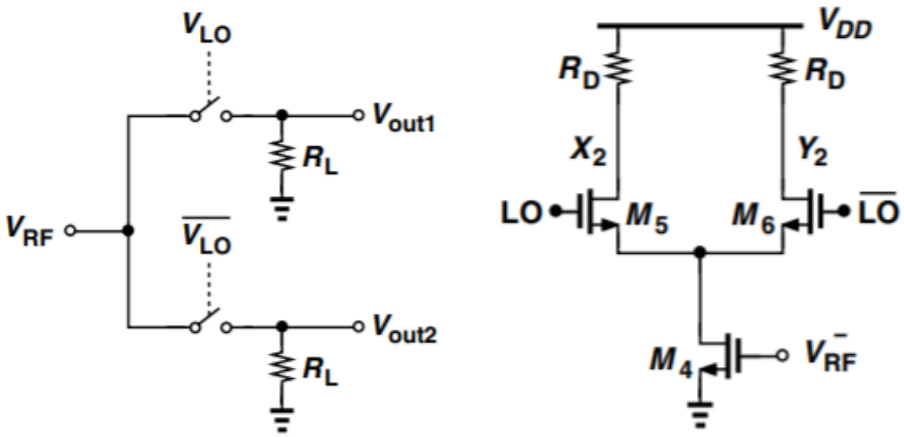

(a) Single-balanced passive mixer. **(b)** Single-balanced active mixer.

Figure 2.6: Examples of single-balanced mixer topologies [17].

As for the double-balanced mixers, the circuit in Figure 2.7(b) is a Gilbert Cell mixer, the most generally used type of mixer. Compared to the single-balanced counterpart, these circuits have a differential transconductance stage in addition to the differential switching stage. This leads to a better isolation between the output port and both of the inputs, theoretically nullifying both feedthroughs if the circuit is fully symmetric. The gain is applied on the RF signal, while the other four transistors are switching both modulated currents from the first stage. In order to have good switching, the transistors in the first stage must be considerably bigger than the four switching transistors.

Once again, the use of source degeneration with an inductor can improve the linearity of the design, and at the same time, have a positive impact to the NF [20]. For example in [21], the Gilbert Cell topology is implemented with an inductive degenerated source, common mode inductor and the gates of the transistors also have an inductive load, while also biasing it at the minimum NF current density bias. This, and the fact that an IF buffer is present and impedance matched to 50 Ω, lowers the total noise and is shown to improve linearity [21].

Another case is the design developed in [22], where the resistive output load is exchanged for an LC tank designed to resonate at the desired frequency of 5 GHz, allowing for an improved headroom and the control of the output bandwidth depending on its quality factor. A common source inductor is used, just like in [21], for common mode rejection of imbalances inherent to asymmetries. An inductor is

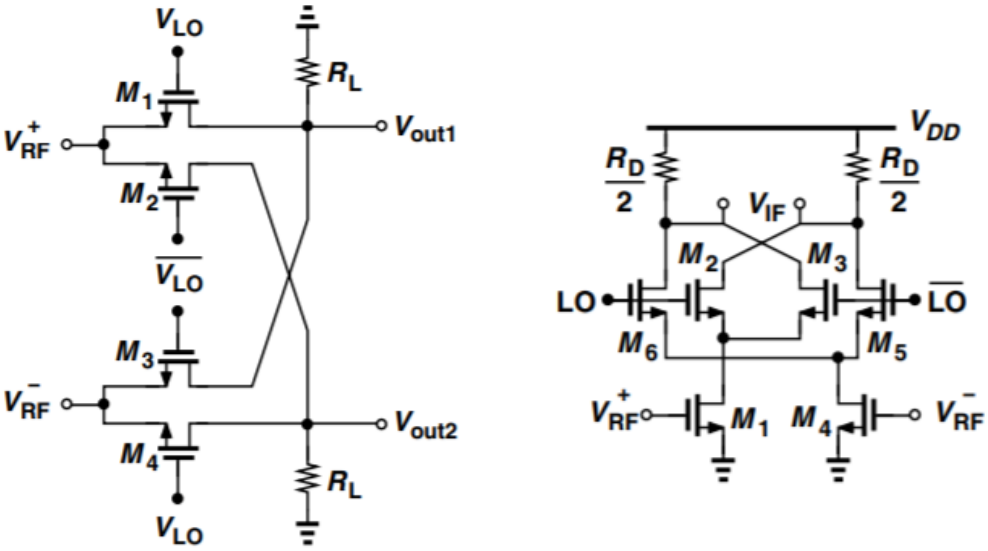

(a) Double-balanced passive mixer. **(b)** Double-balanced active mixer.

Figure 2.7: Examples of double-balanced mixer topologies [17].

also placed between each switching pair and the transconductance stage pair to improve the conversion gain, since they minimize parasitic capacitances. The final circuit can be seen in Figure 2.8.

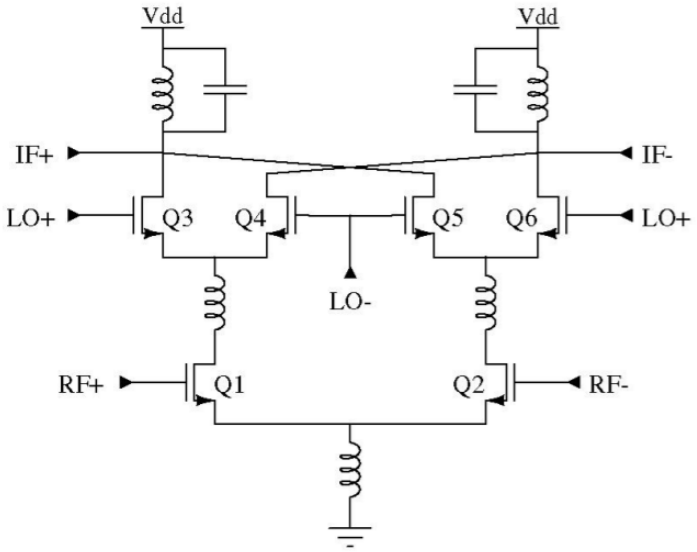

Figure 2.8: Double-balanced mixer design presented in [22].

Although it greatly improves noise and gain, this type of circuit is impractical for small technology sizes and applications, since the use of several inductors means a significant area increase. Ideally,

these benefits are achieved without the need for big area passive components.

2.2.3 Switching Tail Current Bias

A major point of introduction of noise to the circuit is the tail current source. A technique used to mitigate this is presented in [23] and [24], with the use of a switching current bias. This technique was adapted from Voltage-Controlled Oscillator (VCO) circuits [25], [26].

This is achieved by having two MOSFET controlled by each of the IF components. With this, the tail current transistors are constantly changing between strong inversion and accumulation regions, allowing for trapped charge carriers to be released [23]. Therefore, the flicker noise is reduced. In Figure 2.9, this implementation is shown by the use of transistors M1 and M2. Additionally, the transistors M11 and M12 are used as DC shifters. This is needed for the higher voltage of the output to be able to effectively regulate the biasing transistor that is activated.

Compared to the previous noise reducing design, there is only two resistors as extra passive components. Since it uses no inductors or capacitors, it is able to take advantage of a slightly lower noise input without a big impact on circuit size.

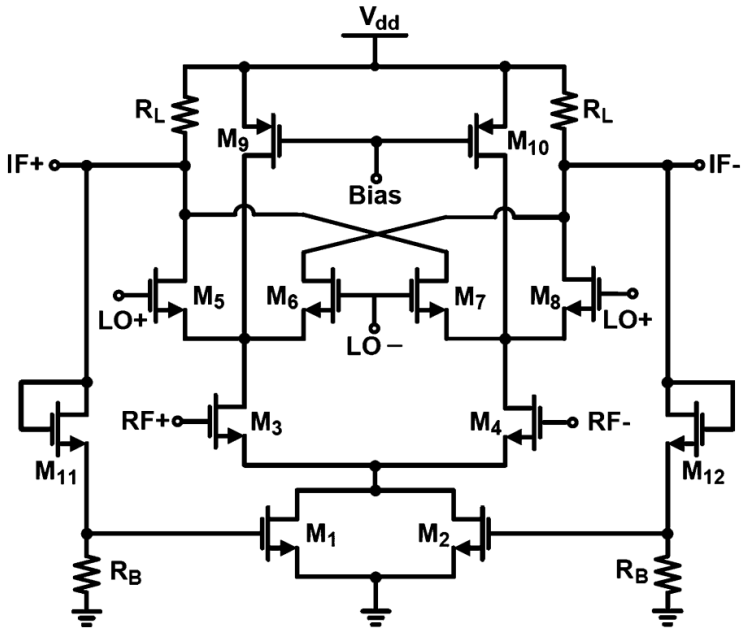

Figure 2.9: Gilbert Cell mixer with switching tail current bias [23]

2.2.4 Balun

For the use of balanced mixers, one or both inputs must be differential. Generally, the signal obtained from the LNA (component before the mixers in Figure 1.1) is single-ended, which is a limitation for the use of double-balanced mixers. This limitation is not limited to the RF port, as the LO can also have a single ended output. Therefore, a balun, or an unbalanced to balanced converter, that has the capability of generating a differential output signal with the corresponding amplitude and phase needed for the balanced mixer from a single ended signal can be used [27].

Stepping momentarily into the discrete components, the most common balun type is the flux coupled balun transformer. Just like a normal transformer, two conductors are winded around a magnetic core, but the side with the input has the other end of the conductor connected to ground, therefore creating an unbalanced condition on the primary winding, while the secondary is in a balanced condition. As shown in Figure 2.10, the secondary winding can also have an optional center tap that is grounded in order to improve the balancing of the output signal. Since it is a transformer, the impedance ratio can also be tuned depending on the number of windings.

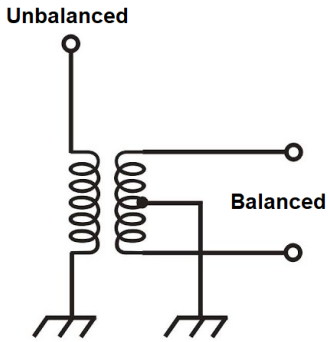

Figure 2.10: Flux coupled balun transformer. Adapted from [27].

Several research has also been conducted on the topic in order to create novel on-chip balun designs using different types of technologies. Some of these new designs are explored in [28] and [29]. In [28], a microstrip-slot-line-microstrip transition is used to create a balun/180° power divider. The design was fabricated on a RO4003c substrate, low-temperature co-fired ceramics (LTCC) and Sapphire, having less than 3 dB of insertion loss across the ultra-broadband range for all of the designs.

Another design is studied in [29], where a Marchand balun circuit is applied in a multi-layer technology. In this application, shown in figure 2.11, the double layer Marchand balun allows for a wider bandwidth and a better coupling coefficient, since the transmission lines are capacitively coupled using overlapping microstrip lines.

Both of the solutions on these articles are smaller than a regular transformer, but their implementation is still on the several millimeter scale.

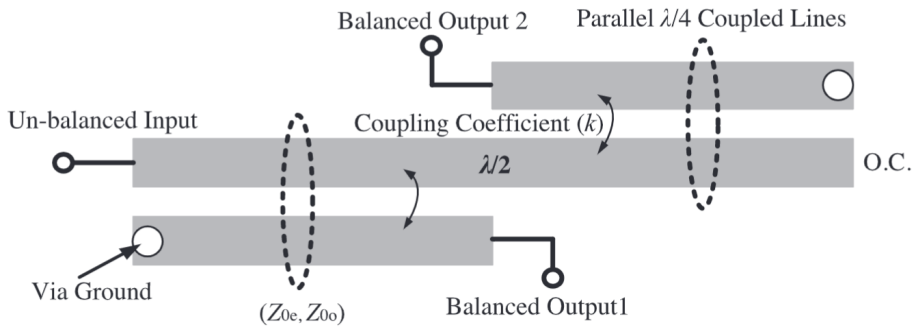

Figure 2.11: Conventional Marchand balun structure [29].

2.3 Relaxation Oscillator

A typical relaxation oscillator is composed of a couple of cross-coupled inverters, a current source for each, two resistive loads and an integrating capacitor, as shown in Figure 2.12.

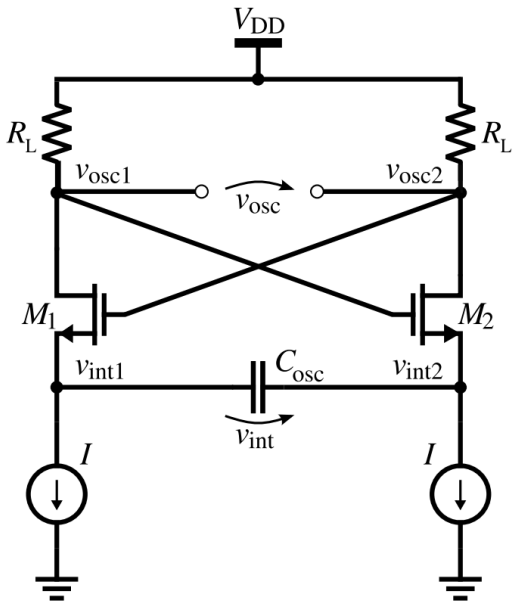

Figure 2.12: Example of CMOS relaxation oscillator [30].

In such oscillator, each inverter is active independently. As the current is integrated, the voltage across the capacitor rises, leading to the latching of the inverters and switching the inverter that is active. After this, the capacitor is discharged, leading to the latch back to the original inverter.

This constant oscillation behaviour is tuned by the size of the resistive load and the capacitor [30],

with an approximate frequency of

$$\mathsf{f}_{osc} = \frac{1}{8 \times \mathsf{C}_{osc} \times \mathsf{R}_L}, \tag{2.11}$$

while the amplitude is dependent on the resistive load and the current sources. Since the circuit switches periodically with latches, the output waveform is a differential square waveform.

Concluding, in order to obtain an oscillation frequency of the desired magnitude for the LO, the passive components require unreasonably large values for the technology used. To prevent this and still be able to use this topology of oscillator, the resistors can be switched for transistors in the triode region, allowing the tuning of its internal resistance to a greater value than a resistor, while having significantly lower area. By doing this, the size of the capacitor can also be lowered, granting the ability of having a low frequency oscillator, with reduced area size, on a nm scale technology.

In the next chapter, this knowledge will be applied to the development of a mixer and an oscillator that can perform desirably for the pulsar receiver.

3

Circuit Development

Contents

Circuit Development

The receiver block (mixer and oscillator), developed in this section, for the receiver envisioned in Brito's thesis [2], was implemented in Cadence using the TSMC65N technology. The development and design choices are discussed below.

3.1 Mixer Design

Taking into account the necessities of this receiver, the mixer developed in this thesis focuses on a low noise application, with good isolation between the ports. As said in chapter 2, pulsar signals have a center frequency of 1 GHz, so that should be the center frequency of the RF port. As for the LO port the desired frequency is 100 kHz. This is because the receiver topology employs a squarer, and the desired pulsar signal should be kept out of its flicker noise region. As the bandwidth of the desired pulsars is lower than 100 kHz, mixing the pulsar signal frequency with the local oscillator will allow it to shift and be kept out of the DC levels of the squarer output. The double balanced mixer, or Gilbert cell, is ideal for this situation. Not only does it have a lower noise floor, but it also has excellent isolation between the ports with its differential inputs and outputs.

The design and simulation of this circuit can be divided in several stages. For initial simplicity's sake, the circuit is tested with an RF input at 1 GHz and the LO frequency of 100 MHz. This allows for better simulation and tuning of the device since it drastically reduces the simulation time, compared to the desired specification of 100 kHz for the LO frequency. After the initial design process, the frequency will be switched to the desired specification.

3.1.1 Ideal Mixer Design

Initially, the circuit can be designed with ideal components from the Cadence libraries. This allows for an initial benchmark of our topology. With the circuit implemented as in figure 3.1 and respective testbench in figure 3.2, the initial DC and transient simulations determine the necessary biasing and power that the transistors need for an optimum operation and gain.

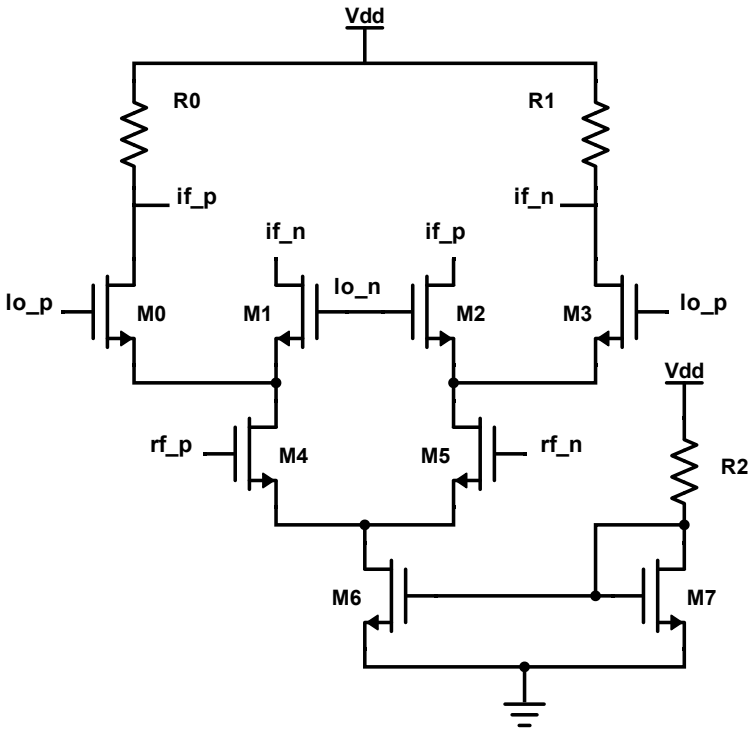

Figure 3.1: Initial ideal mixer schematic.

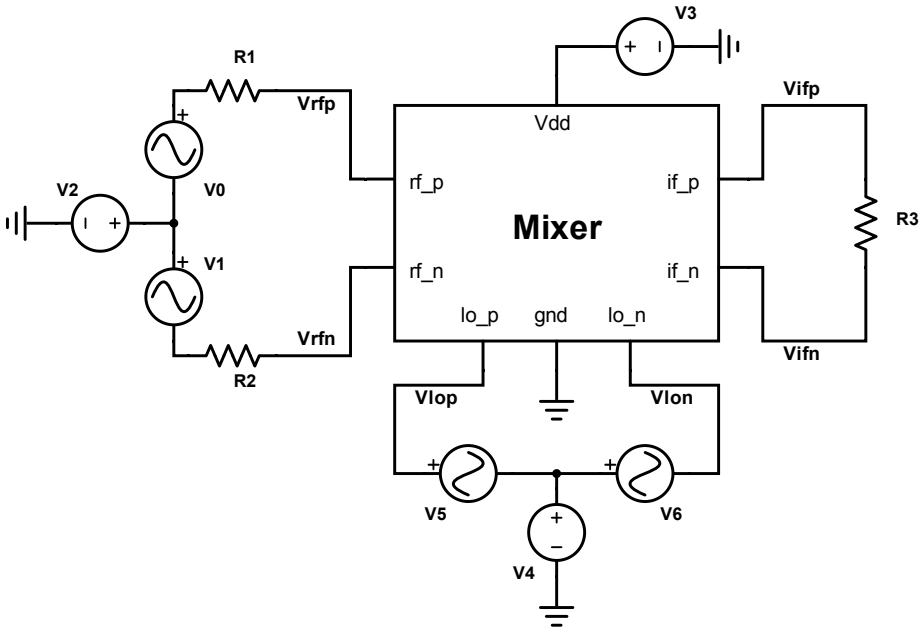

Figure 3.2: Testbench used for the ideal mixer.

Building upon this, the transition to TSMC65N technology components is simplified. A slight adjustment to the component sizes is needed to counteract the parasitic influences of the technology components.

3.1.2 Input Biasing

The test bench in figure 3.2 has the voltage sources V4 and V2 providing the bias, mentioned in table 3.1, for the switching stage MOSFETs and the transconductance stage MOSFETs, respectively. Since these values are not standard in these applications, the mixer circuit must be redesigned for it to have the biasing internally.

Table 3.1: Input DC voltages.

Input	Voltage (V)
VDD	2.5
LO	1.8
RF	1.3

In order to do the biasing internally, a transistor with the drain and the gate shorted can be implemented. This gives a constant voltage output dependant on the size of the transistor and the current input. For the input signal to be filtered a high pass filter is used, in the way of a series capacitor, to block the DC component. This method is shown in figure 3.3.

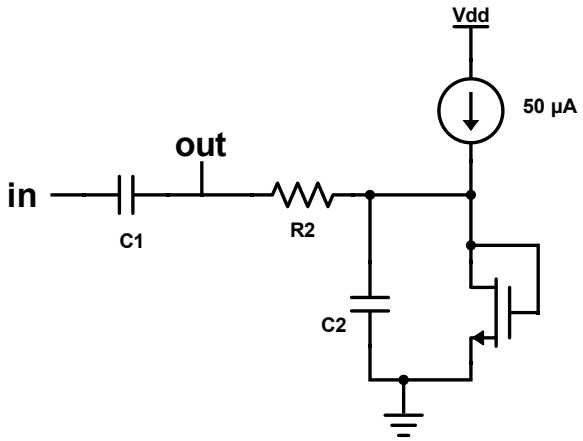

Figure 3.3: Biasing transistor.

In order to only have one external current to provide the biasing for the MOSFETs, therefore reducing the external components, cascading this voltage reference circuit seems feasible, as the bias voltage for the transconductance stage is lower than for the switching stage. However, the current from one input signal that influences the I_D current in the MOSFET, and therefore its voltage drop, would also influence the current in the MOSFET for the other signals, reducing the signal to noise ratio, since there

would be leakage from one input port to the other. Because of this the inputs biasing filter consists of four independent voltage references, two for the RF port (one for each complementary signal of the differential source) and the other two for the LO port (one for each complementary signal of the differential input of the LO).

3.1.3 Switching Mixer Current Bias

The use of capacitors or inductors leads to a trade-off in size for the benefit of noise output. To minimize the noise while also keeping high area, passive components out of the circuit, the switching tail current bias technique is used, as seen in [23] and [24]. In addition to the switching MOSFETs, four other MOSFETs are used in order to shift the output voltage to the threshold of the bias MOSFETs. This can be seen in figure 3.4. The sizing of the transistors used is shown in table 3.2. As for the resistors, each has a value of 500 Ω.

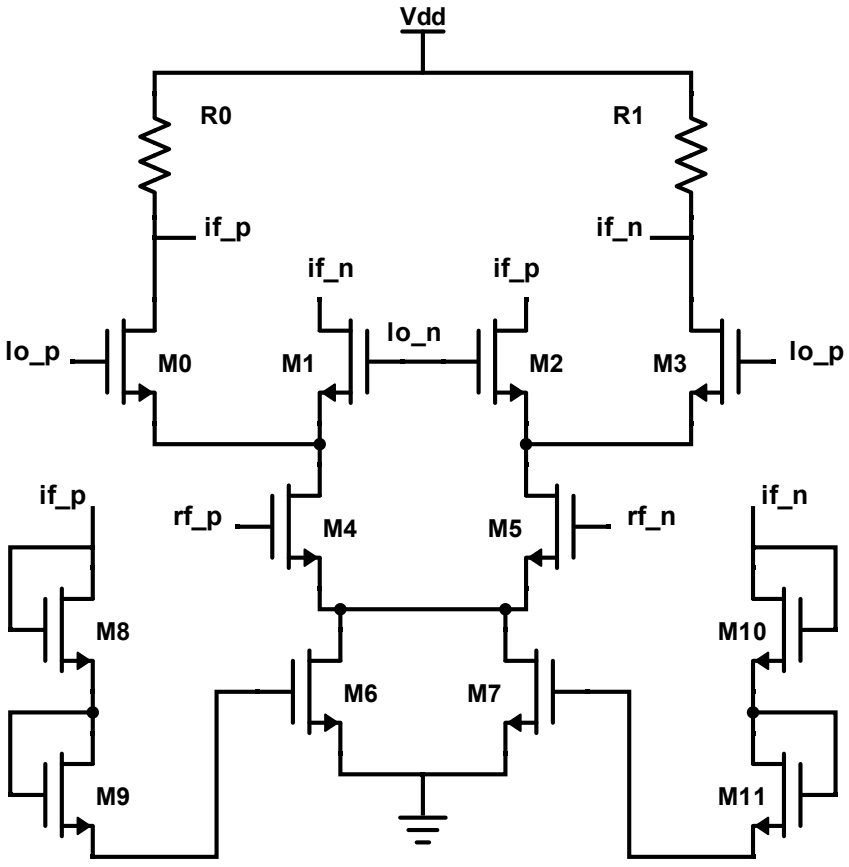

Figure 3.4: Mixer adapted with the switching bias.

Table 3.2: Mixer transistor sizes.

Transistor	**Width** (μm)	**Length** (μm)
M0-M3	20.0	0.280
M4-M5	42.0	0.280
M6-M7	30.0	0.300
M8-M11	1.00	0.400

3.1.4 Desired LO Frequency

Switching to this frequency adds to the complexity of the simulation, since the difference between the two inputs is extremely high. The circuit shown in figure 3.3, at this low of a frequency, also blocks the signal. Considering that it is also connected to the impedance of the switching transistors (M0 to M3), it is not working as a high-pass filter, but as a band-pass filter, which is not desirable.

This can be fixed by adjusting the values of the passive components of the filter, however, that would lead to a significant increase in area for the passive components, all while still being highly dependant on parasitic values of the transistor. Another solution to this is proposed in the next section, with the development of an oscillator that allows the bypassing of said biasing filter.

3.2 Relaxation Oscillator

To counter the LO biasing blocking the signal at the desired frequency for the oscillator, the integration of a simple, slow (for this technology size) oscillator is proposed. The type of oscillator is a relaxation oscillator, as discussed in chapter 2. The final schematic implemented is shown in figure 3.5, with transistors M5 and M11 acting as a resistive load to allow a higher impedance, which is 263.2 kΩ. The transistor and passive component sizes for the oscillator are presented in tables 3.3 and 3.4, respectively.

Since the output of an oscillator of this topology is a square wave, to minimize the impact of the harmonics on the input of the mixer, an RC low-pass filter is implemented with a cutoff frequency at 200 kHz. Since the oscillator is tuned for 100 kHz, this filter minimizes the first odd harmonic (since it is a squared wave) by 6 dB.

Table 3.3: Relaxation oscillator transistor sizes.

Transistor	**Width** (μm)	**Length** (μm)
M0-M1	5.00	1.00
M2-M5	2.00	0.300
M6-M9	0.400	0.280

Table 3.4: Relaxation oscillator passive component sizes.

Component	**Width** (μm)	**Length** (μm)	**Capacitance** (pF)	**Resistance** (kΩ)
C0	50.0	50.0	5.10	-
C1-C2	25.0	50.0	2.55	-
R0-R1	0.400	210	-	400
R2	0.400	231	-	440

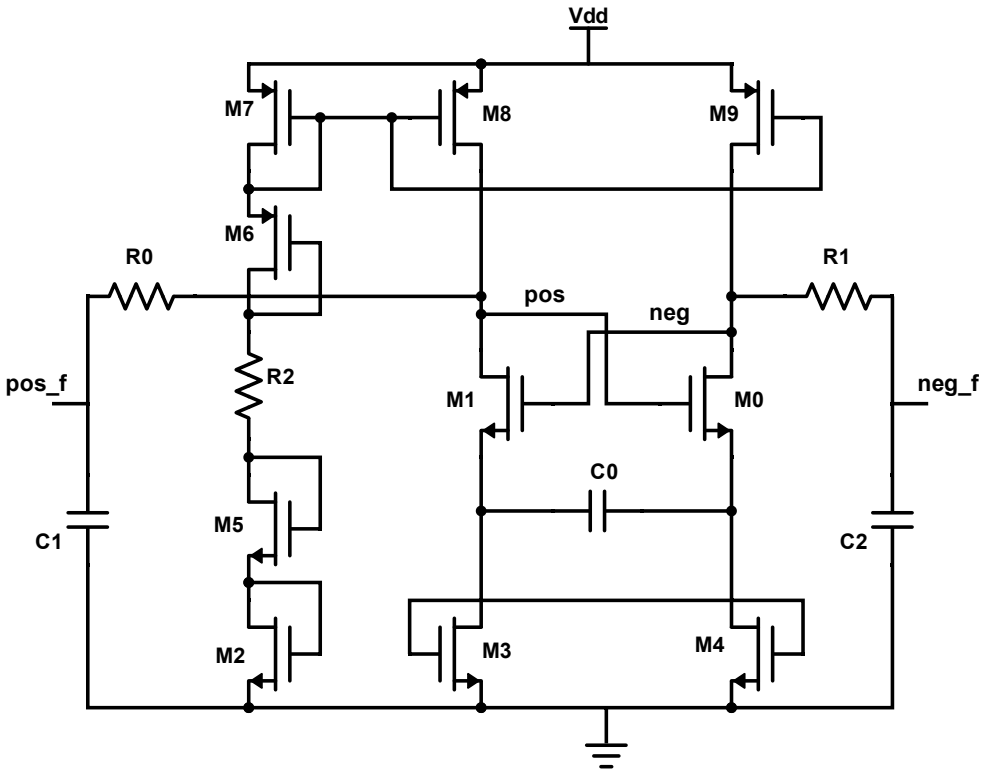

Figure 3.5: Relaxation oscillator schematic.

3.3 Final Design

Using the relaxation oscillator developed as the LO input of the mixer adapted with the switching bias, and the DC biasing transistor for the RF port input biasing, the finished circuit design is presented in figure 3.6. The addition of the oscillator allows the mixer to work at the intended frequency, without the need for filtering at the LO port, since the correct voltage bias is already set by the oscillator. This leads to the use of a biasing filter only at the RF port, where there is minimal loss of alternate current (AC) signal since the input frequencies are much higher than the filter cut-off frequency. The component sizes and values for the input biasing are presented in table 3.5, with the positive and negative input biasing

components having the same sizes, an advantage for symmetry.

Table 3.5: Input biasing component sizes.

Component	**Width** (μm)	**Length** (μm)	**Capacitance** (fF)	**Resistance** (kΩ)
C1-C2	20.0	6.00	253	-
C3-C4	12.0	12.0	299	-
R1-R2	2.00	20.0	-	7.00
M1-M2	0.400	0.600	-	-

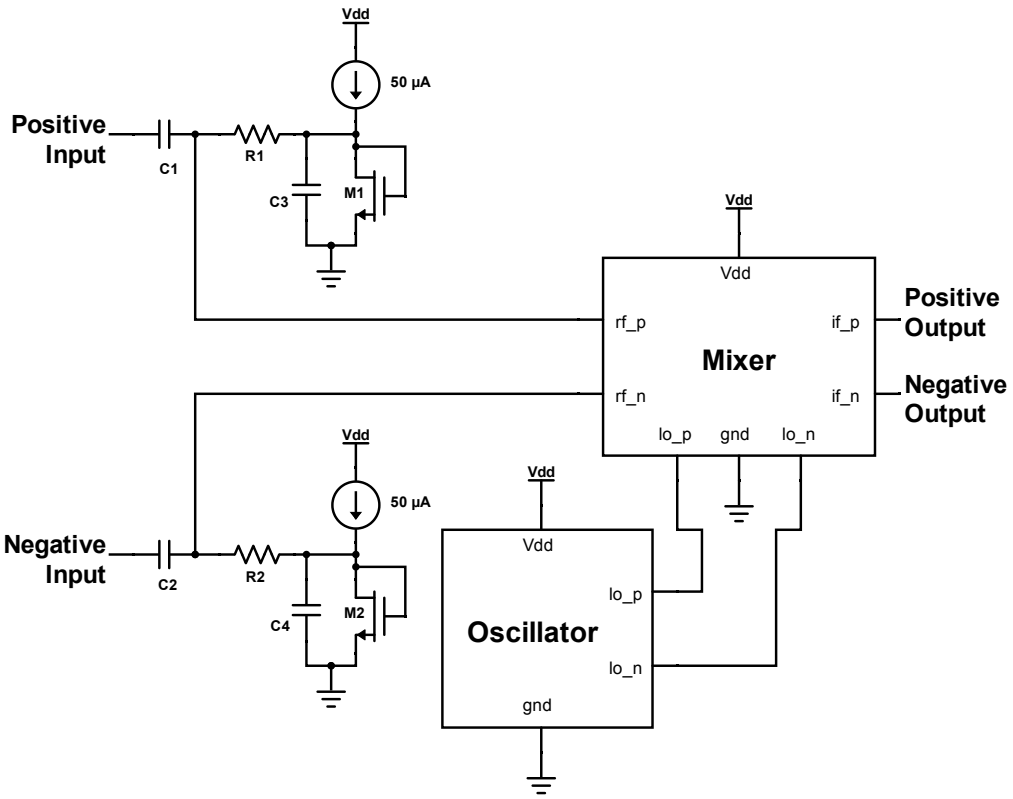

Figure 3.6: Full circuit implementation.

In the next chapter the different circuit simulations are presented with the specifications of each individual circuit, as well as, additional insight on the results and their impact.

4

Results

Contents

Results

In this section, the simulation steps and results of the various development phases for each component are presented. The metrics of the whole system are also presented at the end. These results were obtained using Cadence and the the Spectre RF simulation tools. Due to the nature of the circuit and the discrepancy between the two frequencies, challenges arise. With a higher frequency for the LO, allows for transient simulations to be performed in a timely manner. For the lower, final frequency, this is not possible and the use of Spectre RF analysis using harmonic balance was necessary, since the PSS or QPSS were not able to converge. This is most likely caused by the use of an oscillator that is not ideal.

4.1 Mixer at High LO Frequency

Simulating the circuit shown in figure 3.4 with a transient, the correct functionality of the mixer is verified. Table 4.1 summarizes the defined values of the design variables used for the simulation.

Table 4.1: Transient simulation variables

Variable	Value
V_{LO}	500 mV
V_{RF}	10 mV
f_{LO}	100 MHz
f_{RF}	1 GHz

The simulated results for the mixer, including the input filters and the switching bias, can be seen in figure 4.1. A slight attenuation of the RF is present, due to the biasing circuit. The LO signal also is affected by this attenuation but, later on, with the addition of the developed oscillator, this is not present anymore. The IF output has the two sinusoidal waves with the two frequencies visible.

The arbitrary voltage for the LO must be optimized. To determine the LO amplitude for maximum gain, a voltage sweep is performed. From figure 4.2 it is visible that the 0.5 V used is close to the maximum gain of the circuit designed, just below the 3 dB figure.

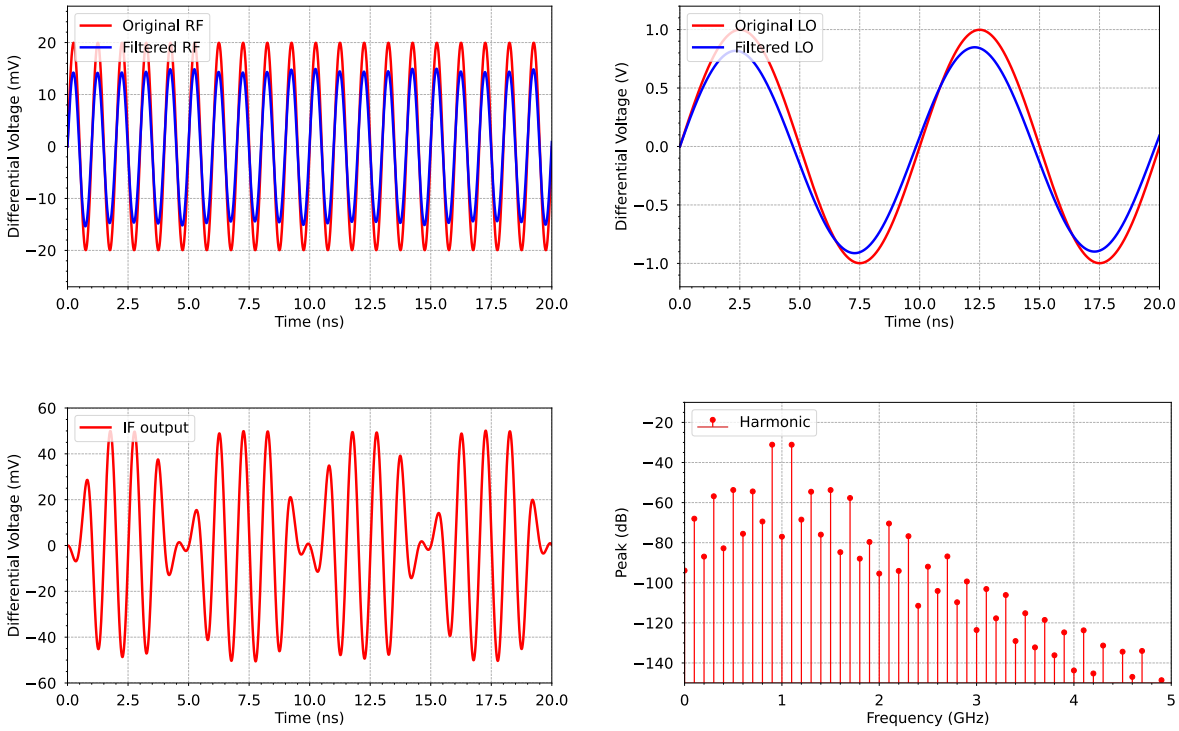

Figure 4.1: Mixer transient simulated response

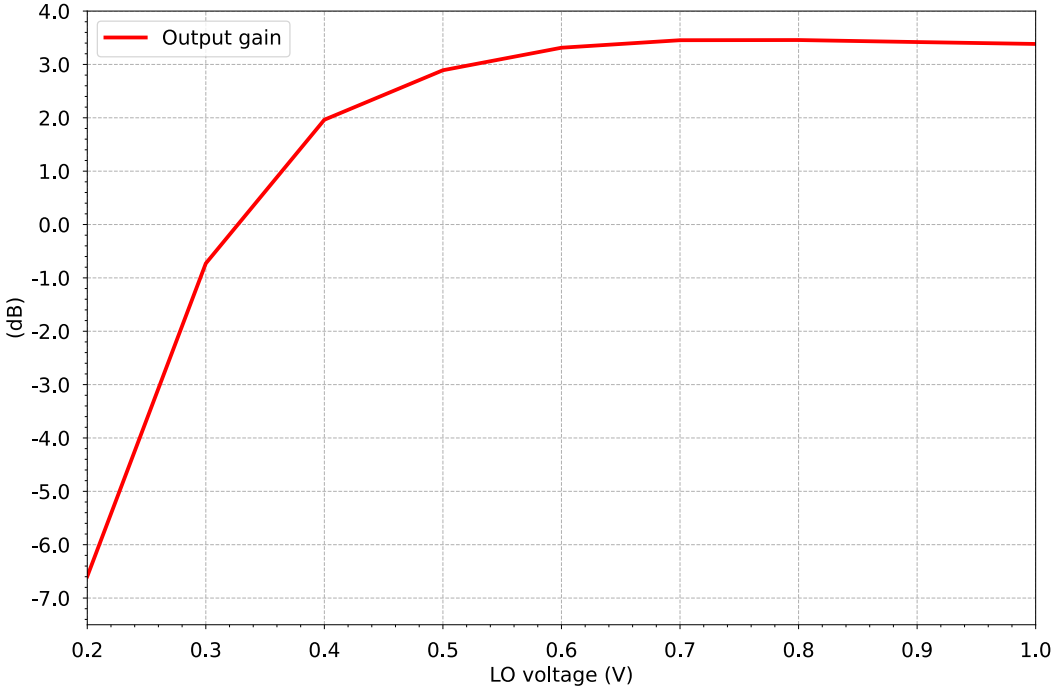

Figure 4.2: Mixer gain in function of LO voltage amplitude.

Once again, these seem to be within the expected specification, allowing the advancement to the final characteristics of the circuit's implementation, which means simulating with 100 kHz at the LO port.

4.2 Mixer at Low LO Frequency

As mentioned in chapter 3, the transition to a lower LO frequency leads to a big attenuation on that port. The effects of this attenuation can be seen in figure 4.3, where the initial 1 V differential oscillator signal is attenuated to 15 mV due to the filter used. This leads to the design choice of bypassing the filter by implementing the oscillator with desired frequency and output DC bias.

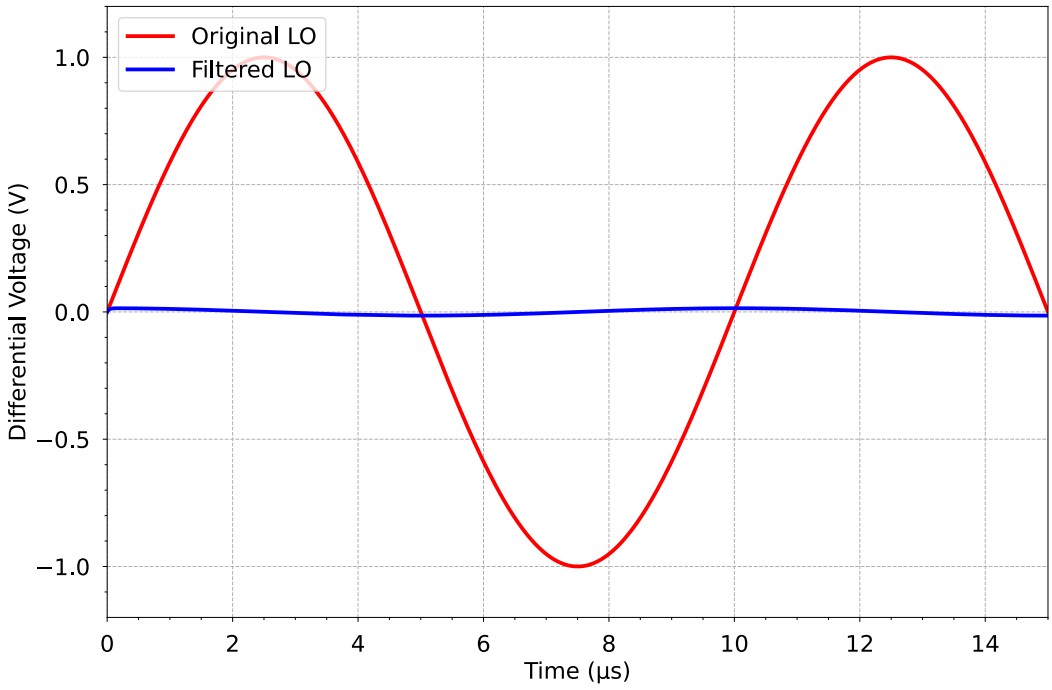

Figure 4.3: Mixer gain in function of LO voltage amplitude.

4.3 Oscillator

From the transient simulations of the oscillator circuit, analyzing a single-ended output in figure 4.4, it can be observed that the oscillator is tuned to an amplitude of 0.6 V centered at 1.9 V. This amplitude value is slightly higher than the necessary to guarantee that the gain is consistently at its maximum, which was around 0.5 V. The 1.9 V DC biasing corresponds to the voltage needed at LO port for the switching transistors to function in the correct operating region. The frequency is also at a value of 106 kHz.

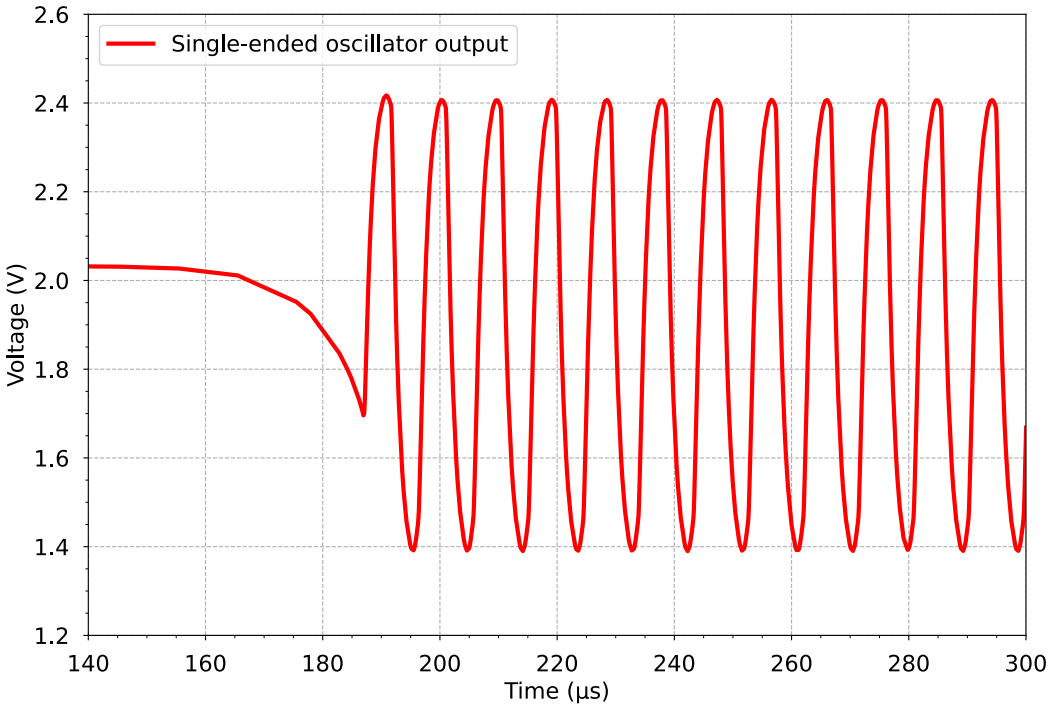

Figure 4.4: Relaxation oscillator single-ended output voltage.

Performing a Monte Carlo simulation with 200 runs, presented in figure 4.5, the mean frequency continues at the 106 kHz mark, but with a standard deviation of 23 kHz. Although undesirable, such variation in frequency due to production and mismatch will not affect the final functionality of the mixer. That is because the signal from the pulsar is not a sine wave, but a periodic pulse. The objective of the mixer is just to shift this signal a few kHz out of what will be the squarer's DC output. Therefore, a frequency deviation of around 20 kHz at the oscillator, leads to a deviation on the shift caused by the mixer to the RF port. Although, even if the shift to the pulsar signal is a 80 kHz or a 120 kHz shift, it will still keep the signal out if the flicker noise region generated at the squarer's transistors and the band-pass filter following the squarer (figure 1.1) can be tuned to cope with this shift as well.

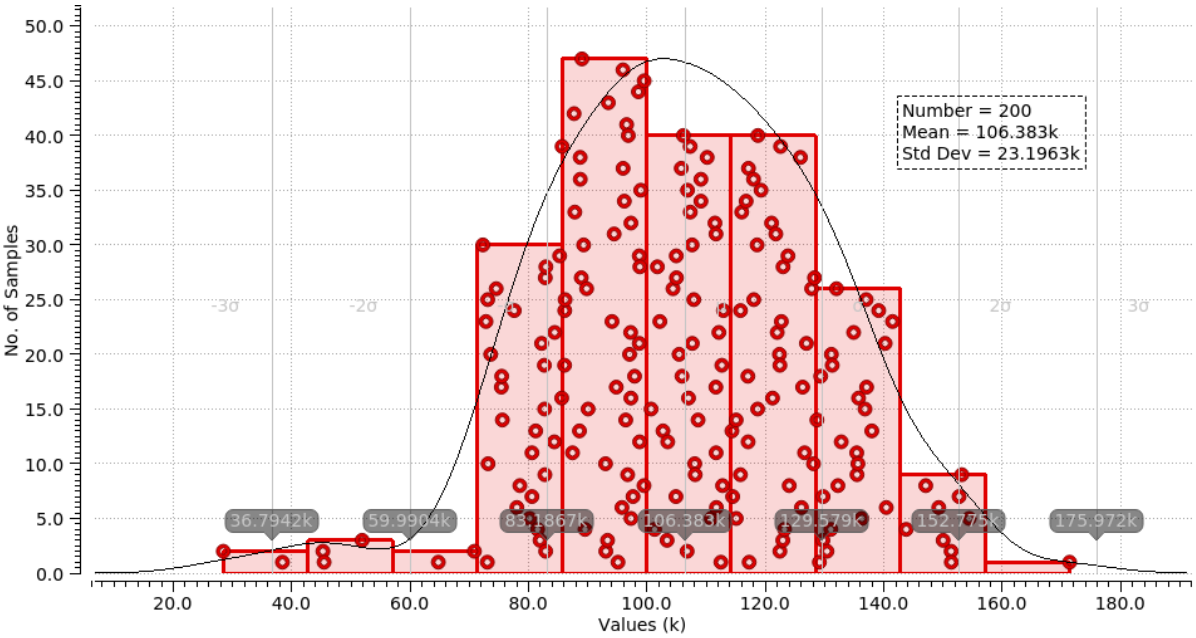

Figure 4.5: Relaxation oscillator frequency Monte Carlo.

Figure 4.6(a), a transient of the oscillator output before and after RC filter, shows the difference in output waveform due to the RC filter. The harmonics are attenuated and the output signal is closer to a sine wave. This can be seen in the Fast Fourier Transform (FFT) shown in figure 4.6(b), where the third harmonic is -16 dB in relation to the 100 kHz harmonic, 6 dB lower than the circuit without a filter.

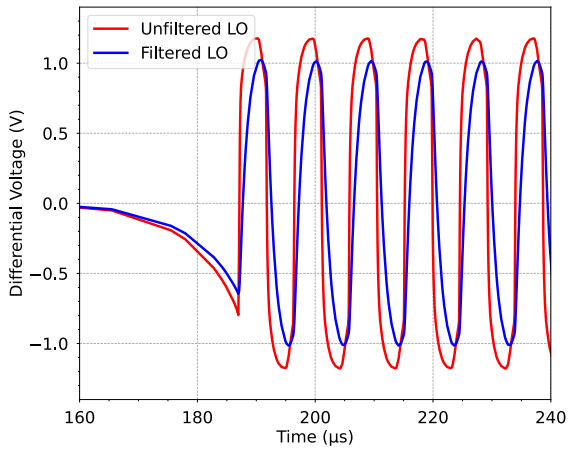

(a) Transient voltage output.

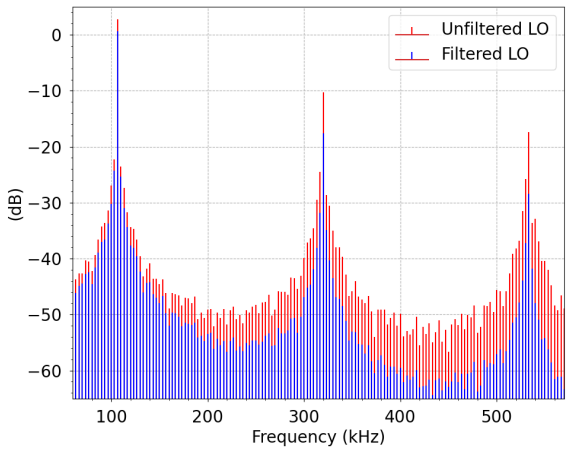

(b) Output FFT.

Figure 4.6: RC filter influence on relaxation oscillator.

4.4 Final Circuit

Connecting the relaxation oscillator directly to the LO port of the frequency mixer without the biasing filter before the switching pair transistors, the circuit is on its final form. From the simulation of the output gain in relation to the frequency, shown in figure 4.7, the final circuit obtained a maximum gain of 4.5 dB, with a bandwidth of 7.3 GHz. Focusing on the pulsar signal frequency and bandwidth, from the zoomed in section in the figure, the gain is nearly constant at 4.5 dB between 800 MHz and 1.2 GHz.

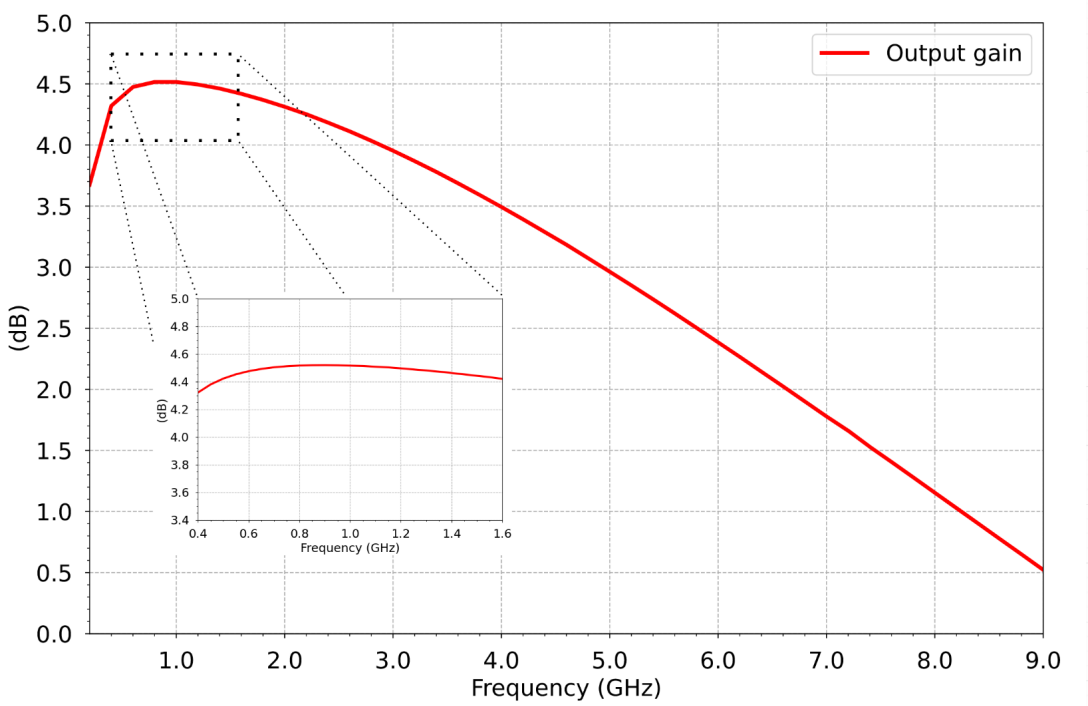

Figure 4.7: Circuit output gain and bandwidth.

The 1_{dB} compression point of the circuit is simulated to -9.5 dBm, as shown in figure 4.8, meaning that the input power can reach that value before the output gain decreases by 1 dB. Since the pulsar signals will be of very reduced power, this result is well within the desired specifications. Although the expected use of this receiver is with pulsar signals with power below the noise level, the 1_{dB} compression point result obtained allows for the future possibility of using the circuit at closer ranges to the pulsars than expected.

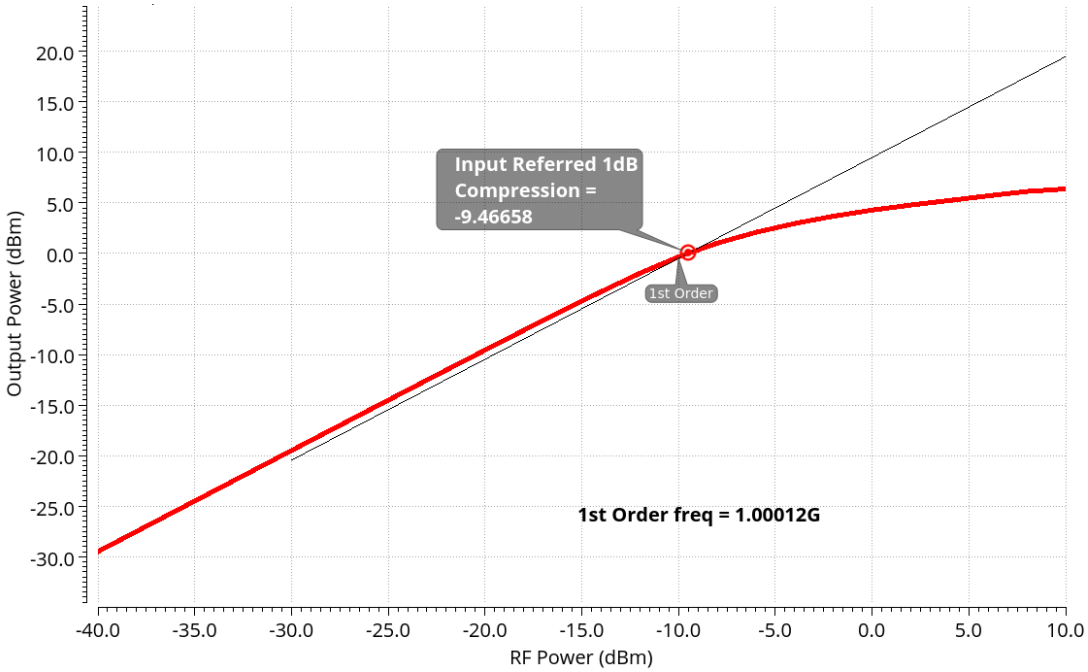

Figure 4.8: Circuit 1_{dB} compression point.

Although the simulations were simplified by using the pulsar input as sine waves, the results obtained, and presented in this chapter, demonstrate that the circuit is able to mix two signals with different magnitudes of frequency, at a low power level and with a gain of 4.5 dB. These specifications were obtained through several iterations and tuning cycles, obtaining a mixer and local oscillator that can be integrated into the receiver envisioned in [2].

5

Conclusions and Future Work

Conclusions and Future Work

The desire and importance of outer space navigation are undeniable to understand the universe and explore its contents. The use and development of new localization and navigation systems is essential to allow better and further exploration. The benefit of pulsars for this application is still a relatively new research area, but with promising results.

In order to take advantage of pulsar signals for navigation, the development of capable receivers is necessary. The work proposed for this thesis, a mixer and oscillator for a quadratic receiver topology, was achieved.

The Gilbert Cell mixer with switching current bias developed achieves a gain of 4.5 dB, 1_{dB} compression point of -9.5 dBm. The 7.3 GHz input bandwidth makes it suitable for the application, especially since the maximum gain is constant at the pulsar signal's frequency. As for the relaxation oscillator, it boasts an amplitude of 0.6 V and a frequency of 106 kHz. The development of these topologies at these frequencies was quite challenging for a small and fast technology such as the TSMC65N.

This result allows the squarer of the receiver to perform its objective without introducing flicker noise to the pulsar signal. Since the mixer is able to function correctly with both inputs having frequencies orders of magnitude apart, the desired shift of the pulsar signal by a few 100 kHz allows the ADC to have a higher resolution. Such objective was the main difficulty of this project, which, although functional, still has some deviation on the oscillator frequency. Even though it does not affect the functionality of the final product, it implies some extra steps at the data processing stage.

The presented results validate the proposed topologies but some improvements in hardware are still possible. An external interface to regulate the relaxation oscillator's capacitance could minimize the frequency deviation. For future work, the fabrication layout and simulation should also be finalized. The integration of the squarer into this design should be analyzed, as it may allow the reduction of conversions between current and voltage. Finally, the rest of the receiver can be implemented as a single tape-out integrated circuit.

Bibliography

[1] S. Asmar, D. Firre, A. Accomazzo, A. Bhanji, P. Ferri, J. Hudiburg, P. Liebrecht, G. Morse, and G. Mann, "NASA's and ESA's Tracking Networks, A Decade of Strategic Partnership for Solar System Exploration," *2018 SpaceOps Conference*, 2018. [Online]. Available: https://doi.org/10.2514/6.2018-2430

[2] Brito, Diogo, "Radio Pulsar System for Navigation," Ph.D. dissertation, Instituto Superior Técnico, 2018.

[3] S. Rüster, "The Phase Diagram of Neutral Quark Matter," Ph.D. dissertation, December 2006.

[4] D. Matsakis, J. Taylor, and M. Eubanks, "A Statistic for Describing Pulsar and Clock Stabilities," *Astronomy and Astrophysics*, vol. 326, Septemper 1997. [Online]. Available: https://articles.adsabs.harvard.edu/pdf/1997A%26A...326..924M

[5] A. Lyne and F. Graham-Smith, *Pulsar Astronomy*, 4th ed., ser. Cambridge Astrophysics. Cambridge University Press, 2012. [Online]. Available: https://doi.org/10.1017/CBO9780511844584

[6] R. S. Lynch, "Pulsar Timing Arrays," *Journal of Physics: Conference Series*, vol. 610, may 2015. [Online]. Available: https://doi.org/10.1088/1742-6596/610/1/012017

[7] Australia Telescope National Facility. (2022) The ATNF Pulsar Catalogue. [Online]. Available: https://www.atnf.csiro.au/research/pulsar/psrcat/

[8] D. Brito, G. Tavares, J. Fernandes, A. Noroozi, and C. Verhoeven, "Radio Pulsar Receiver Systems for Space Navigation," 2015. [Online]. Available: https://www.researchgate.net/publication/280085456

[9] D. R. Lorimer and M. Kramer, *Handbook of Pulsar Astronomy*, 2012. [Online]. Available: https://ui.adsabs.harvard.edu/abs/2012hpa..book.....L

[10] J. Hessels, B. Stappers, A. Alexov, T. Coenen, T. Hassall, A. Karastergiou, V. Kondratiev, M. Kramer, J. Leeuwen, J. Mol, A. Noutsos, and P. Weltevrede, "Early Pulsar Observations with LOFAR," Septemper 2010. [Online]. Available: https://hdl.handle.net/11245/1.336415

[11] J. Santos, D. Brito, G. Tavares, and J. Fernandes, “Radio Pulsar Signal Generator,” in *2018 IEEE International Symposium on Circuits and Systems (ISCAS)*, 2018. [Online]. Available: https://doi.org/10.1109/ISCAS.2018.8351229

[12] S. I. Sheikh, *The use of variable celestial X-ray sources for spacecraft navigation*. University of Maryland, College Park, 2005.

[13] T. F. L. Collaboration, “An extremely bright gamma-ray pulsar in the Large Magellanic Cloud,” *Science*, vol. 350, 2015. [Online]. Available: https://www.science.org/doi/abs/10.1126/science.aac7400

[14] N. Luo, L.-p. Xu, H. Zhang, and Q. Xie, “Feasibility analysis for attitude estimation based on pulsar polarization measurement,” *Journal of Zhejiang University SCIENCE C*, vol. 14, 06 2013. [Online]. Available: https://doi.org/10.1631/jzus.C1200291

[15] J. Sala-alvarez, A. Planas, J. Villares, R. Estalella, and J. Paredes, “Feasibility Study for a Spacecraft Navigation System relying on Pulsar Timing Information,” 01 2004. [Online]. Available: http://hdl.handle.net/2117/11514

[16] T. H. Lee, *The Design of CMOS Radio-Frequency Integrated Circuits*, 2nd ed. Cambridge University Press, 2003.

[17] B. Razavi, *Rf Microelectronics*. Prentice Hall, 1998.

[18] M. Rahman and R. Harjani, “A Sub-1-V 194-µW 31-dB FOM 2.3–2.5-GHz Mixer-First Receiver Frontend for WBAN With Mutual Noise Cancellation,” *IEEE Transactions on Microwave Theory and Techniques*, vol. 64, 2016. [Online]. Available: https://doi.org/10.1109/TMTT.2016.2536603

[19] C. Marki and F. Marki, “Mixer Basics Primer,” Tech. Rep., 2010. [Online]. Available: https://www.aspen-electronics.com/uploads/3/7/1/2/37123419/mixer_basics_primer-min.pdf

[20] K. L. Fong and R. Meyer, “Monolithic rf active mixer design,” *IEEE Transactions on Circuits and Systems II: Analog and Digital Signal Processing*, vol. 46, 1999. [Online]. Available: https://doi.org/10.1109/82.754857

[21] K. Tang, M. Khanpour, P. Garcia, C. Garnier, and S. Voinigescu, “65-nm cmos, w-band receivers for imaging applications,” in *2007 IEEE Custom Integrated Circuits Conference*, 2007. [Online]. Available: https://doi.org/10.1109/CICC.2007.4405838

[22] D. Alldred, B. Cousins, and S. P. Voinigescu, “A 1.2v, 60-ghz radio receiver with on-chip transformers and inductors in 90-nm cmos,” in *2006 IEEE Compound Semiconductor Integrated Circuit Symposium*, 2006. [Online]. Available: https://doi.org/10.1109/CSICS.2006.319876

[23] J.-H. Kim, H.-W. An, and T.-Y. Yun, “A low-noise wlan mixer using switched biasing technique,” *IEEE Microwave and Wireless Components Letters*, vol. 19, 2009. [Online]. Available: https://doi.org/10.1109/LMWC.2009.2029746

[24] S. Rout and K. Sethi, “Design of high gain and low noise cmos gilbert cell mixer for receiver front end design,” 2016. [Online]. Available: https://doi.org/10.1109/ICIT.2016.014

[25] E. Klumperink, S. Gierkink, A. van der Wel, and B. Nauta, “Reducing MOSFET 1/f noise and power consumption by switched biasing,” *IEEE Journal of Solid-State Circuits*, vol. 35, 2000. [Online]. Available: https://doi.org/10.1109/4.848208

[26] C. Boon, M. Do, K. Yeo, J. Ma, and X. Zhang, “RF CMOS low-phase-noise LC oscillator through memory reduction tail transistor,” *IEEE Transactions on Circuits and Systems II: Express Briefs*, vol. 51, 2004. [Online]. Available: https://doi.org/10.1109/TCSII.2003.821519

[27] C. Marki and D. Jorgesen, “Balun Basics Primer,” Tech. Rep., 2014. [Online]. Available: https://www.aspen-electronics.com/uploads/3/7/1/2/37123419/balun_basics_primer-min.pdf

[28] A. K. Poddar, U. L. Rohde, V. Madhavan, and S. K. Koul, “A novel uwb balun: Application in 5g systems,” in *2016 IEEE International Frequency Control Symposium (IFCS)*, 2016. [Online]. Available: https://doi.org/10.1109/FCS.2016.7546747

[29] R. T. Hammed, “Compact marchand balun circuit for uwb application,” *AEU - International Journal of Electronics and Communications*, 2015. [Online]. Available: https://doi.org/10.1016/j.aeue.2015.02.005

[30] Ortigueira, Eduardo, “Low Phase-Noise CMOS RC Oscillator for RF Applications,” Ph.D. dissertation, Universidade Nova de Lisboa, 2018. [Online]. Available: http://hdl.handle.net/10362/28407